Effect of Ligand−Metal Interactions on the Growth of Transition-Metal and Alloy Nanoparticles

Anna C. S. Samia,[†] John A. Schlueter,[‡] J. Samuel Jiang,[‡] Samuel D. Bader,[‡] Chang-Jin Qin,[§] and Xiao-Min Lin*[,†,‡,||]

Chemistry Division, Materials Science Division, and Center for Nanoscale Materials, Argonne National Laboratory, Argonne, Illinois 60439 and Department of Chemistry, University of Chicago, 5635 South Ellis Avenue, Chicago, Illinois 60637

Received May 7, 2006. Revised Manuscript Received August 6, 2006

The growth of cobalt, iron, and platinum and their alloy nanoparticles was investigated with oleic acid and trioctylphosphine oxide as ligands. Both the ligand type and concentration are important in determining the final product of the reactions. With a high concentration of oleic acid, thermal decomposition of dicobalt octacarbonyl and iron pentacarbonyl precursors yields only molecular cluster complex species with oxidized metal centers. However, reduction of platinum acetylacetonate under identical conditions yields nanometer-sized particles. In the presence of a high concentration of trioctylphosphine oxide, only the cobalt system was observed to form a cluster−complex species, while both the iron and platinum systems form nanometer-sized particles. This oxidation process, which forms cluster complexes, provides a digestive ripening mechanism that competes with the Ostwald ripening process, thus affecting the particle size and composition of both the pure metal and alloy nanoparticles.

Introduction

Transition-metal nanoparticles have attracted great attention due to their unique size-dependent magnetic properties and potential applications in a diverse range of areas including catalysis, sensors, and drug delivery.[1−4] In particular, chemically synthesized transition-metal alloy nanoparticles, such as FePt and CoPt, have been studied extensively because of their high magnetocrystalline anisotropy and chemical stability. These unique properties make them possible candidates for the next generation of magnetic storage media and high-performance permanent magnets.[5,6] To realize these potentials it is extremely important to develop synthetic methods that yield monodispersed magnetic nanoparticles of tunable size, shape, and composition.[7] Over the past few years several successful solution-phase syntheses for Co,[1,8] Fe,[9] Co_xPt_{1-x},[10,11] Fe_xPt_{1-x},[12,13] and $Fe_xCo_yPt_{1-x-y}$[14] nanoparticles have been developed that can provide crystalline particles with controllable morphology and narrow size distribution. The essence of these syntheses is the thermal decomposition of organometallic precursors or reduction of metal salts in the presence of several long-chain acid, amine, phosphine, or phosphine oxide ligands. Typically, two types of ligands, one strongly bound to the metal surface and another loosely bound, are employed in order to adjust the growth rate of the nanoparticles while maintaining the size monodispersity during the reaction.[1] Although these syntheses have been studied extensively by many groups, there are still lingering questions regarding the role of the chemical ligands on particle growth. For instance, FePt nanoparticles synthesized according to the procedure developed by Sun et al.[12] typically do not grow beyond certain sizes, as the Ostwald ripening mechanism would predict. The only way to tune the final particle size is through adjustment of the reaction rate, which changes the overall number of nucleation sites.[13] For metal alloy magnetic nanoparticles the ability to control the particle composition is also very important because binary alloys typically form a continuous range of solid solutions with both stoichiometric and nonstoichiometric compositions.[15] The crystal structure, electronic structure, and magnetic properties depend not only on the particle size and shape but also on the relative ratio of the alloying components.[16−18] It was

* To whom correspondence should be addressed. E-mail: xmlin@anl.gov.
[†] Chemistry Division, Argonne National Laboratory.
[‡] Materials Science Division, Argonne National Laboratory.
[§] University of Chicago.
[||] Center for Nanoscale Materials, Argonne National Laboratory.

(1) Murray, C. B.; Sun, S.; Doyle, H.; Betley, T. *MRS Bull.* **2001**, *26*, 985−991.
(2) Narayanan, R.; El-Sayed, M. A. *J. Phys. Chem. B* **2005**, *109*, 12663−12676.
(3) Li, G. X.; Wang, S. X.; Sun, S. H. *IEEE Trans. Magn.* **2004**, *40*, 3000−3002.
(4) Ito, A.; Shinkai, M.; Honda, H.; Kobayashi, T. *J. Biosci. Bioeng.* **2005**, *100*, 1−11.
(5) Weller, D.; Moser, A. *IEEE Trans. Magn.* **1999**, *35*, 4423−4439.
(6) Zeng, H.; Li, J.; Liu, J. P.; Wang, Z. L.; Sun, S. *Nature* **2002**, 420, 395−398.
(7) Hyeon, T. *Chem. Commun.* **2003**, *8*, 927−934.
(8) Puntes, V. F.; Krishnan, K. M.; Alivisatos, A. P. *Science* **2001**, *291*, 2115−2117.
(9) Park, S.-J.; Kim, S.; Lee, S.; Khim, Z. G.; Char, K.; Hyeon, T. *J. Am. Chem. Soc.* **2000**, *122*, 8581−8582.
(10) Park, J.; Kim, M. G.; Jun, Y.-W.; Lee, J. S.; Lee, W.-R.; Cheon, J. *J. Am. Chem. Soc.* **2004**, *126*, 9072−9078.
(11) Shevchenko, E. V.; Talapin, D. V.; Rogach, A. L.; Kornowski, A.; Haase, M.; Weller, H. *J. Am. Chem. Soc.* **2002**, *124*, 11480−11485.
(12) Sun, S.; Murray, C. B.; Weller, D.; Folks, L.; Moser, A. *Science* **2000**, *287*, 1989−1992.
(13) Chen, M.; Liu, J. P.; Sun, S. *J. Am. Chem. Soc.* **2004**, *126*, 8394−8395.
(14) Chen, M.; Nikles, D. E. *Nano Lett.* **2002**, *2*, 211−214.
(15) Massalski, T. *Binary Alloy Phase Diagrams*; American Society for Metals: Metals Park, OH, 1990; Vol. 2.

10.1021/cm0610579 CCC: $33.50
Published on Web 09/27/2006

found that the molar ratio of Fe (or Co) to Pt in the final alloy nanoparticle is much less than the same molar ratio in the precursor reagents. This was attributed to high volatility of the carbonyl precursors.[12,19] However, it is difficult to explain the fact that nearly one-half of the Fe or Co precursor is lost in these syntheses through this argument.

To address these issues, the ligand−metal interactions, especially during the initial nucleation stage, have to be understood further. We recently demonstrated that the presence of excess oleic acid (OA) ligand during the organometallic synthesis of magnetic cobalt nanoparticles results in particle growth inhibition and disintegration of large nanoparticles in favor of molecular cluster complexes.[20] These results show that a simple picture of surface ligands acting merely as passivating agents to prevent particle agglomeration is not adequate in these reactions. Instead, surface ligands play a much more active role in controlling the particle growth kinetics, which ultimately affects the particle size, shape, and composition. In this paper, we extend our previous work to investigate the effects of two commonly used ligands, namely, OA and trioctylphosphine oxide (TOPO), on the decomposition of iron and cobalt carbonyl precursors and on the reduction of platinum acetylacetonate in order to gain insights on how the specific ligand−metal interactions affect the nucleation and growth of pure transition metals and their alloy nanoparticles. We focus our study on the scenario in which the ligand concentration is much higher than the metal precursor so that the effect of the ligand is amplified and becomes a dominant factor in determining the reaction pathway.

Experimental Section

Chemicals and Materials. Iron pentacarbonyl, $Fe(CO)_5$ (99.99+%), platinum acetylacetonate, $Pt(acac)_2$, (97%), oleic acid (OA, 99+%), trioctylphosphine oxide (TOPO, 99%), 1,2-hexadecanediol (tech. 90%), octyl ether (99%), anhydrous methanol (99.8%), anhydrous toluene (99%), and anhydrous 1,2-dichlorobenzene (99%) were purchased from Aldrich and used as received. Dicobalt octacarbonyl ($Co_2(CO)_8$) precursor (stabilized in 1−5% hexane) was obtained from Alfa Aesar, and hexane was removed through evaporation inside a glove box that had less than 1 ppm oxygen and moisture. The transmission electron microscopy (TEM) grids with supported holy carbon film were purchased from Electron Microscopy Sciences.

Synthesis. All syntheses and postreaction processing were carried out in an argon atmosphere using standard glove box and Schlenk line techniques in a well-ventilated hood. (Note: carbonyl precursors decompose with the evolution of carbon monoxide. This is a toxic gas that must be efficiently vented.) The concentration of metal precursors used in our synthesis is dictated by their solubility in the solvent. The concentration of cobalt and platinum used in the following synthesis is close to its upper solubility limit. The iron concentration is selected to be twice the platinum concentration.

For all experiments involving only a single metal precursor, the relative concentration of the reagents was kept consistent with the metal-to-ligand molar ratio maintained at 1:2.5. The metal precursors were introduced with the reaction temperature set at 100 °C, followed by reflux heating at the boiling point of the solvent mixture. The reflux heating time for all reactions is kept at 30 min unless specified otherwise. To investigate the ligand interaction with Co, 1.58 mmol of $Co_2(CO)_8$ was dissolved in 2 mL of anhydrous 1,2-dichlorobenzene and then rapidly injected into a solution of 20 mL of octyl ether containing either 7.9 mmol of TOPO or OA. The refluxing temperature is 265 °C due to the large volume of low boiling point 1,2-dichlorobenzene and oleic acid. To study the ligand interactions with Fe, 1.48 mmol of $Fe(CO)_5$ was rapidly injected into the solution of 20 mL of octyl ether containing either 3.7 mmol of TOPO or OA at 100 °C, followed by reflux heating at 286 °C for 30 min. In the case of the reduction of the platinum precursor, 0.7 mmol of $Pt(acac)_2$ and 2.1 mmol of 1,2-hexadecanediol were dissolved into 20 mL of octyl ether together with 1.75 mmol of TOPO or OA and reflux heated at 286 °C for 30 min.

In a similar approach, the bimetallic iron− and cobalt−platinum nanoparticles were prepared based on a slightly modified synthesis developed by Sun et al.[12] In a typical experiment, $Pt(acac)_2$ (0.7 mmol, 0.2750 g), 1,2-hexadecanediol (2.1 mmol, 0.5430 g), and TOPO (3.7 mmol, 1.4310 g) or OA (3.7 mmol, 1.17 mL) were dissolved in 20 mL of octyl ether and heated to 100 °C. Then, $Fe(CO)_5$ (1.48 mmol, 200 μL) or $Co_2(CO)_8$ (0.74 mmol, 0.2530 g dissolved in 2 mL of anhydrous 1,2-dichlorobenzene) was rapidly injected into the reaction mixture, and the resulting mixture was heated to reflux at 286 °C for 30 min. The mixture was cooled to room temperature, and the nanoparticles were precipitated with the addition of 2 mL of anhydrous toluene followed by 20 mL of anhydrous methanol. Following centrifugation, the isolated nanoparticles were redispersed in anhydrous toluene (20 mL) and reprecipitated with anhydrous methanol (20 mL). This washing and centrifugation step was repeated once more, and the precipitated nanoparticle powder was dried under vacuum for further analysis. Elemental analyses of the isolated nanoparticles were conducted at Galbraith Laboratory, Inc.

Transmission Electron Microscopy. TEM studies were conducted on the as-prepared nanoparticles using a Philips CM30 at a 200 kV acceleration voltage. A typical sample was prepared by depositing a droplet of a diluted colloid solution of the nanoparticles onto a holy carbon grid and allowing the solvent to evaporate. High-resolution TEM studies were performed on a JEOL 4000EX with a 400 kV acceleration voltage.

Magnetic Measurements. The magnetic properties of the nanoparticles were investigated using a Quantum Design MPMS-5S superconducting quantum interference device (SQUID) magnetometer with magnetic fields of up to 5 T. For all the stable colloidal solutions the samples were first mixed with didodecyldimethylammonium bromide (DDAB) and the solvent was subsequently removed to obtain a powder sample. Addition of DDAB helps to separate the particles so the magnetic properties measured are close to the properties of intrinsic isolated particles. In the case when the as-prepared sample precipitates immediately, magnetic measurements were done on the precipitated powder directly after being washed and dried. Annealing of the alloy sample was done using a powder sample, and subsequent magnetic measurements were done on the annealed powder. The temperature-dependent magnetization curves were measured after cooling the sample to 2 K either in a zero magnetic field (zero-field-cooled, i.e., ZFC) or in a 100 Oe magnetic field (field-cooled, i.e., FC). The magnetic susceptibility was subsequently measured in an applied field of 100 Oe as the sample warms up. For superparamagnetic nanoparticles, ZFC and FC curves typically diverge below a characteristic

(16) Klemmer, T. J. et al. *Appl. Phys. Lett.* **2002**, *81*, 2220−2222.
(17) Stahl, B. et al. *Phys. Rev. B* **2003,** *67*, 014422−014434.
(18) Ulmeanu, M.; Antoniak, C.; Wiedwald, U.; Farle, M.; Frait, Z.; Sun, S. *Phys. Rev. B* **2004,** *69*, 054417−054423.
(19) Sun, S.; Fullerton, E. E.; Weller, D.; Murray, C. B. *IEEE. Trans. Magn.* **2001**, *37*, 1239−1243.
(20) Samia, A. C. S.; Hyzer, K.; Schlueter, J. A.; Qin, C.-J.; Jiang, J. S.; Bader, S. D.; Lin, X.-M. *J. Am. Chem. Soc.* **2005**, *127*, 4126−4127.

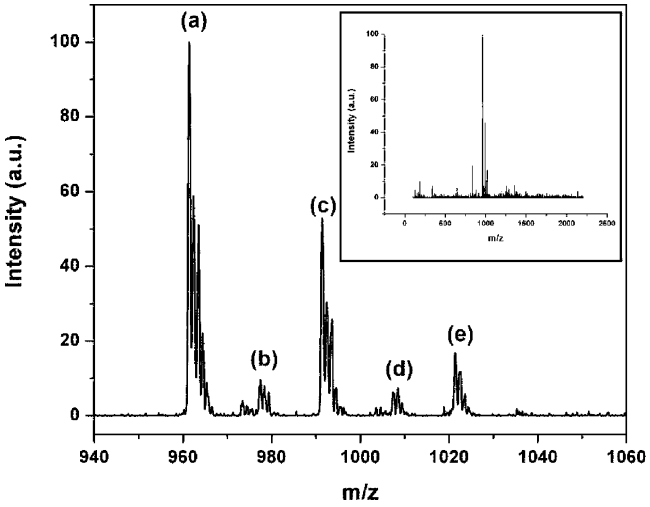

Figure 1. ESI-MS spectrum of Co−OA cluster complexes in octyl ether (with a fragmentation voltage of 200 V) and methanol as carrier solvent. The mass of the peaks correspond to (a) $[Co(II)_2(C_{18}H_{33}O_2)_3]^+$, (b) $[Co(II)_2(C_{18}H_{33}O_2)_3O]^+$, (c) $[Co(I)_2(C_{18}H_{33}O_2)_3CO + 2H]^+$, (d) $[Co(I)_2(C_{18}H_{33}O_2)_3OCO + 2H]^+$, and (e) $[Co(I)_3(C_{18}H_{33}O_2)_3 + H]^+$. The inset shows the entire mass range from 0 to 2250.

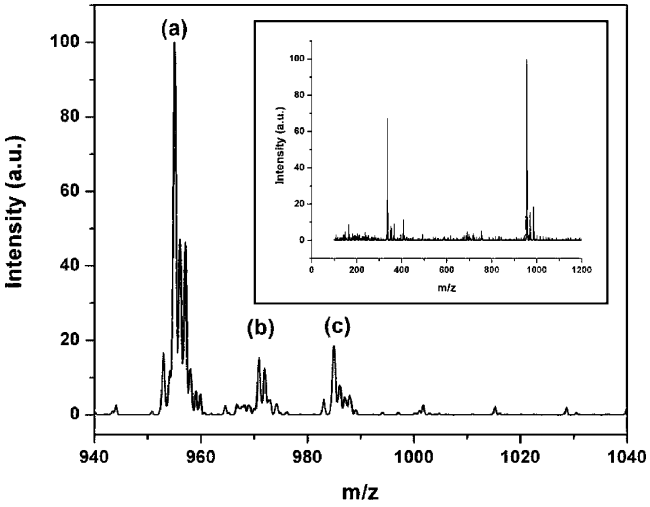

Figure 2. ESI-MS spectrum of Fe−OA cluster solution (with 250 V fragmentation voltages) with methanol as carrier solvent. Two main groups of ions detected are $Fe_2(OA)_3$ (*m*/*z* at 955−985) and FeOA clusters (*m*/*z* at 337−367). The main panel shows the zoomed in $Fe_2(OA)_3$ region, with mass of each ion corresponding to (a) $[Fe(II)_2(C_{18}H_{33}O_2)_3]^+$, (b) $[Fe(II)_2(C_{18}H_{33}O_2)_3O]^+$, and (c) $[Fe(I)_2(C_{18}H_{33}O_2)_3CO + 2H]^+$. The inset shows the entire mass range from 0 to 1200.

temperature (blocking temperature, T_B), which depend on both the magnetic anisotropy and the average size of the particles.[21]

Powder X-ray Diffractometry. X-ray diffraction (XRD) data were collected using a Rigaku X-ray powder diffractometer, which utilizes Kα radiation from a Cu target.

Mass Spectrometry. Electrospray ionization mass spectrometry (ESI-MS) measurements were conducted using an Agilent 1100 LC/MSD mass spectrometer equipped with an ESI ion source. The mass spectra were collected through flow injection under different fragmentation voltages (70−400 V) using either methanol or ethanol as carrier solvent.

Fourier Transform Infrared Spectroscopy (FTIR). FTIR spectra were collected using a Bruker Vertex 70 spectrometer equipped with a mercury cadmium telluride (MCT) detector and a Pike ATR accessory.

Results and Discussions

Ligand Effects on Transition-Metal Nanoparticles. With a high concentration of ligand, a variety of reaction products are formed during the thermal decomposition and reduction of the different organometallic precursors. The nature of the species formed indicates the different binding strengths between the ligands (OA, TOPO) and metals (Fe, Co, Pt).

Case for Oleic Acid. Upon injection of $Co_2(CO)_8$ into the octyl ether solution containing OA at 100 °C, the reaction mixture quickly turned black but eventually transformed to a clear violet-blue solution after reflux heating. TEM analysis showed no nanometer-sized particles in this solution. ESI-MS studies were conducted at different fragmentation voltages to analyze the components of this violet solution. Figure 1 is a mass spectrum obtained at 200 V fragmentation voltage using methanol as a carrier solvent. Similar to the sample prepared in dichlorobenzene,[20] the major components detected are a group of ions with mass centered at 990 Da. The isotope pattern indicates that they are +1 charged species with mass corresponding to clusters of Co_2 or Co_3 coordinated with three OA ligand molecules. The metal centers are oxidized with +1 and +2 valence states. Previous studies indicated that the first observed black coloration is due to the initial formation of Co nanoparticles, which were digested into a Co−OA cluster complex upon continuous heating of the reaction mixture at high temperature.[20] Formation of cluster complexes with OA ligand is not limited to Co. Thermal decomposition of $Fe(CO)_5$ and reflux heating under the condition of high concentration of OA yielded a clear yellow solution after 30 min. ESI-MS studies also revealed the presence of similar cluster species in the solution with the main component corresponding to FeOA and $Fe_2(OA)_3$ clusters (Figure 2). In both cases, clusters containing carbonyl groups are also present, indicating partial decomposition of the original precursor under these experimental conditions.

Reduction of $Pt(acac)_2$ with 1,2-hexadecanediol under the same condition did not result in cluster formation. Instead, a solid precipitate was observed. Electron microscopy studies revealed that the precipitate consists of aggregates of Pt nanoparticles (inset in Figure 3a). Both the XRD (Figure 3a) and selected area electron diffraction (SAED) indicate a face-centered-cubic (fcc) phase, the same as for bulk Pt. Using the Scherer equation to analyze the width of X-ray diffraction peaks, an average size of 14 nm is estimated, which is consistent with the direct analysis from the TEM micrograph. Subsequent solvent washing steps were conducted to remove free OA ligands from the precipitated Pt nanoparticles. FTIR measurements on the dried powder sample (Figure 3b) indicated that the remaining ligand molecules bound to the Pt surface exist in oleate form, which induce strong asymmetric ν_{COO^-} peaks at 1594 and 1559 cm^{-1} and a symmetric ν_{COO^-} peak 1407 cm^{-1}, respectively. Unlike the case when OA molecules are chemically absorbed on the surface of Co nanoparticles,[22] a doublet for the asymmetric ν_{COO^-} peaks is clearly resolved. This shows OA

(21) Cullity, B. D. *Introduction to Magnetic Materials*; Addison-Wesley: London, 1972.

(22) Suslick, K. S.; Fang, M.; Hyeon, T. *J. Am Chem. Soc.* **1996**, *118*, 11960−11961.

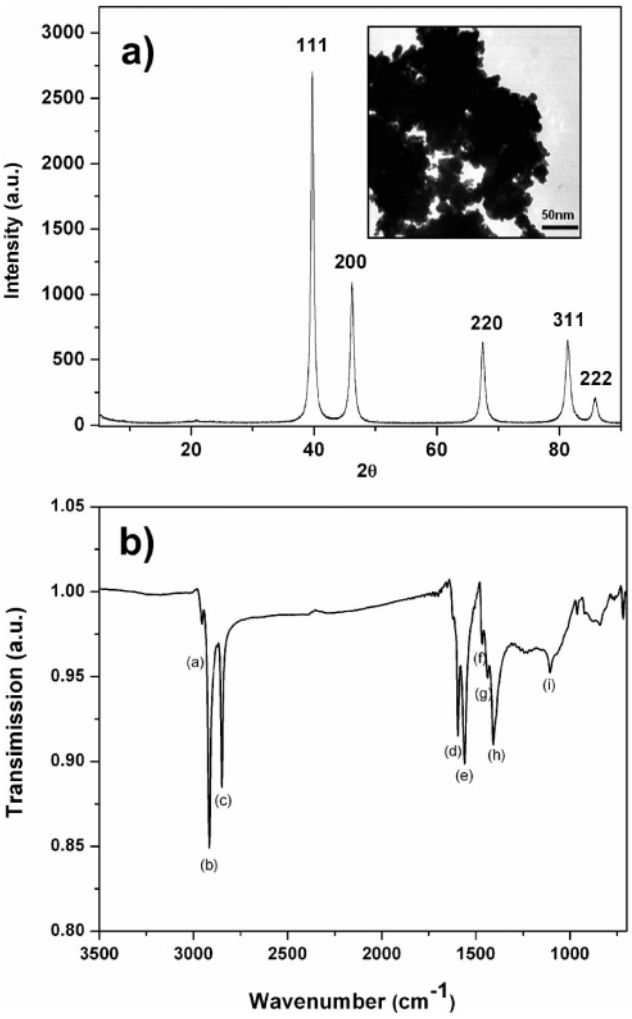

Figure 3. a) XRD pattern of the Pt nanoparticles obtained in the presence of excess OA. The inset is a TEM image of the precipitated nanoparticles. b) FTIR spectra of Pt nanoparticle powder after precipitation and a solvent wash. Absorption peak (a) at 2955 cm^{-1} is due to C−H stretching in terminal CH_3. Peaks at (b) 2916 and (c) 2849 cm^{-1} are due to asymmetric and symmetric stretching of the methylene group. Strong asymmetric ν_{COO^-} peaks at (d) 1594 and (e) 1559 cm^{-1} and a symmetric ν_{COO^-} peak at (h) 1407 cm^{-1} indicate oleate formation on platinum surfaces. Peaks at (f) 1466 cm^{-1} and (g) 1437 cm^{-1} are due to C−H bending in methylene groups. Peak at (i) 1107 cm^{-1} could be due to a C−H wagging mode.

molecules are chemically adsorbed on the Pt nanoparticles with two configurations, either as a bridging bidentate form or a form more close to monodentate.[22,23]

A set of controlled experiments were also conducted wherein decomposition of $Co_2(CO)_8$ and $Fe(CO)_5$ was carried out in the presence of 1,2-hexadecanediol and excess OA. Interestingly, the same reducing agent that is capable of reducing $Pt(acac)_2$ did not promote Co or Fe nanoparticle formation, and the metal−OA cluster complex persisted. This demonstrates the high chemical stability of the Co−OA and Fe−OA cluster complexes.

Case for Trioctylphosphine Oxide. The same reactions were carried out using TOPO as ligand instead of OA. Thermal decomposition of $Co_2(CO)_8$ in octyl ether solution with a high concentration of TOPO formed a blue-colored Co−TOPO complex solution. ESI-MS spectra of this solution revealed the presence of Co clusters with a much wider mass distribution, as shown in Figure 4. The isotope pattern indicated a mixture of both +1 and +2 charged species with Co_1, Co_2, and Co_4 metal centers ligated to several TOPO molecules and residual carbonyl groups.

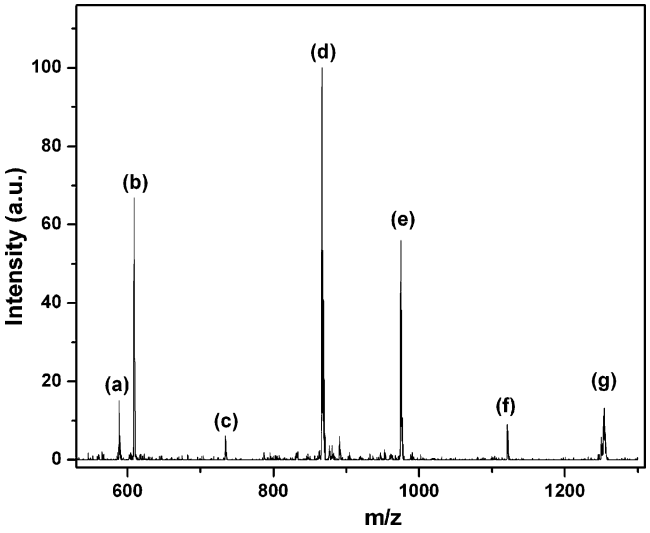

Figure 4. ESI-MS spectrum of cobalt−TOPO complex in octyl ether (with a fragmentation voltage of 200 V) using methanol as carrier solvent. The mass of the main peaks correspond to (a) $[(TOPO)Co(0)Co(I)(CO)_3]^+$, (b) $[(TOPO)_3Co(II)]^{2+}$, (c) $[(TOPO)Co(0)_3Co(I)(CO)_4]^+$, (d) $[(TOPO)_2Co(II)Cl]^+$, (e) $[(TOPO)_2Co(0)Co(I)(CO)_3]^+$, (f) $[(TOPO)_2Co(0)_3Co(I)(CO)_4]^+$, and (g) $[(TOPO)_3Co(II)Cl]^+$. The appearance of chlorine ions in (d) and (g) are likely due to the 1,2-dicholorobenzene solvent used to dissolve the cobalt precursor.

A more distinctive difference between TOPO and OA occurs in the thermal decomposition of $Fe(CO)_5$. Whereas Fe clusters form with OA ligand, no complex formation occurs when TOPO is used. Instead, the reaction mixture remains black even after the solution is refluxed for more than 1 h. Electron microscopy studies confirmed the presence of dispersed nanoparticles in the reaction product with particle sizes ranging from 2 to 10 nm (Figure 5a). High-resolution TEM analysis shows that all particles are crystalline (inset of Figure 5a). Powder X-ray diffraction on a sample exposed to air shows diffraction peaks closer to Fe_3O_4 phase (Figure 5b).

Reduction of $Pt(acac)_2$ with 1,2-hexadecanediol in the presence of TOPO ligands leads to particle precipitation, similar to the case for the OA ligand. Electron microscopy studies reveal that the precipitate consists of aggregates of Pt nanoparticles with an fcc structure (Figure 6). Using the Scherer equation, an average size of 11 nm was estimated from the XRD peaks. The TOPO ligand, however, does not bind strongly to the Pt surface, as indicated by FTIR measurement of the sample after being washed. No IR signal corresponding to the remaining TOPO molecules on the nanoparticle surface was detected.

Ligand Effects on Alloy Nanoparticles. Because various transition metals react differently with OA and TOPO ligands, which is evident from the above experiments, the same effects could ultimately influence formation of FePt and CoPt alloy particles. In the following sections we examine the consequences of using OA or TOPO as ligand in the alloy nanoparticle synthesis.

(23) Wu, N.; Fu, L.; Su, M.; Aslam, M.; Wong, K. C.; Dravid, V. P. *Nano Lett.* **2004**, *4*, 383−386.

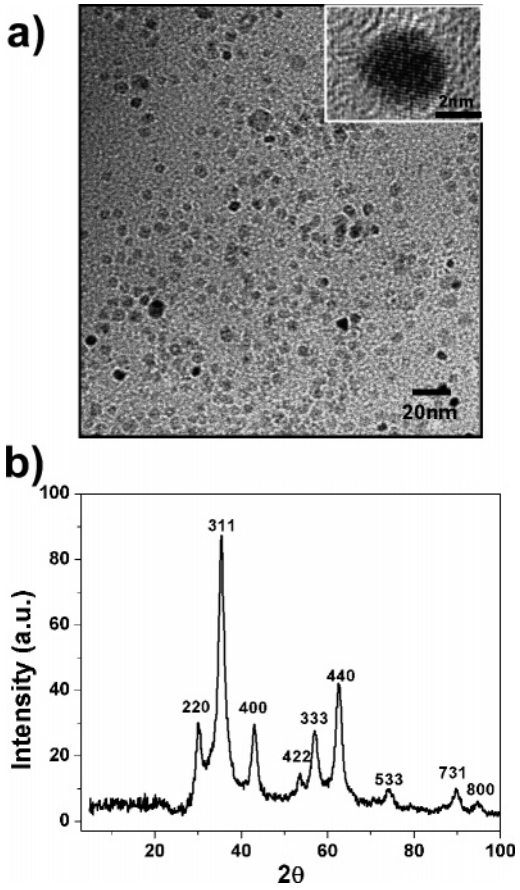

Figure 5. (a) TEM image of the iron nanoparticles with sizes ranging from 2 to 10 nm obtained by thermal decomposition of Fe−carbonyl in the presence of excess TOPO. The inset shows a high-resolution TEM image of a 5 nm nanoparticle. (b) XRD pattern obtained from the TOPO-capped nanoparticles are iron oxide nanoparticles with lattice spacing close to Fe_3O_4.

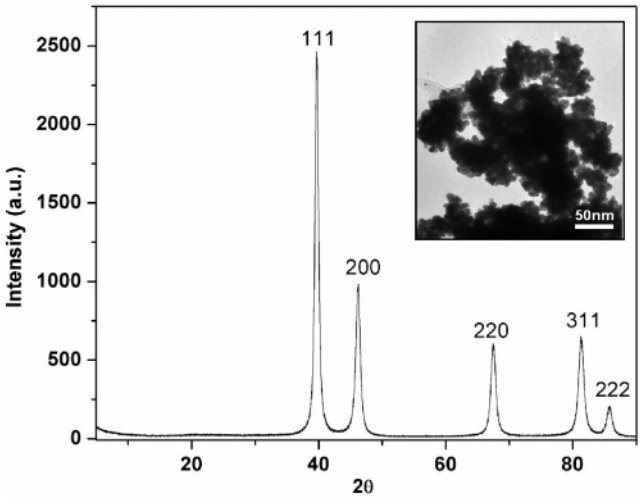

Figure 6. XRD pattern of the Pt nanoparticles obtained in the presence of excess TOPO. The inset is a TEM image of the precipitated nanoparticles.

Iron−Platinum Nanoparticles. Simultaneous thermal decomposition of $Fe(CO)_5$ and reduction of $Pt(acac)_2$ yields highly monodispersed, spherical FePt nanoparticles with an average diameter of 5 nm (Figure 7a) after reflux heating with excess OA molecules for 30 min. High-resolution TEM studies show that the particles are single crystals (Figure 7b). Similar to an earlier report, prolonged heating does not increase the particle size.[13] Chemical analysis of the washed nanoparticle sample using inductively coupled plasma atomic emission spectroscopy (ICP-AES) shows an Fe:Pt molar ratio of 1:1.2, which is much lower than the corresponding molar ratio in the organometallic precursors. XRD analysis reveals that the as-prepared samples adopt an fcc structure, which can be converted to the chemically ordered face-centered-tetragonal (fct) phase upon annealing the sample at 550 °C for 2 h under an inert atmosphere (Figure 7c). Magnetic measurements using a SQUID magnetometer show that the as-prepared 5 nm FePt nanoparticles are superparamagnetic with a blocking temperature of 33 K (Figure 7d). This low blocking temperature is consistent with the low magneto-crystalline anisotropy of the fcc structure and the small particle size. Following the annealing step, the nanoparticles were converted to the fct phase with a higher anisotropy with some degree of particle sintering, both of which led to a large increase in blocking temperature (Figure 7d).

In comparison, use of TOPO as ligand resulted in formation of a bimodal size distribution of FePt particles, which consists of both 2 and 14 nm nanoparticles (Figure 8a). High-resolution TEM studies show that both of these particles are crystalline (Figure 8b). Chemical analysis of the TOPO-capped sample yields an Fe:Pt molar ratio of 1:0.6, which is much closer to the initial ratio of 2:1 in the precursors. The XRD pattern of the as-prepared sample exhibits broad diffraction peaks due to a large population of 2 nm sized particles. The ZFC susceptibility curve of the as-prepared sample shows a series of kinks in the temperature range of 30−100 K (Figure 8d). After annealing the sample at 550 °C for 2 h under an inert atmosphere, a more pronounced fct phase becomes evident in the diffraction pattern (Figure 8c). As a result, the blocking temperature of the annealed sample exceeds room temperature (Figure 8d). This is due to the increase of anisotropy from fcc to fct phase as well as the particle volume increase due to sintering.

Cobalt−Platinum Nanoparticles. Similar to the case of FePt, monodispersed spherical CoPt nanoparticles are obtained using OA as ligand. The average particle diameter is 2 nm, which is much smaller than that of the OA-ligated FePt nanoparticles (Figure 9a). High-resolution TEM studies show that the particles are also crystalline (Figure 9b). Chemical analysis yields a Co:Pt molar ratio of 1:1.5, which is also much smaller than the 2:1 molar ratio in the precursor reagents. XRD analysis reveals that the as-prepared sample has an fcc structure, which can be converted to the chemically ordered fct phase upon annealing the sample at 750 °C for 2 h under an inert atmosphere (Figure 9c). SQUID measurements show that the as-prepared 2 nm CoPt nanoparticles are superparamagnetic with a blocking temperature of 4.5 K (Figure 9d). After being annealed, the nanoparticles sinter and are converted to the high-anisotropy fct phase, which is reflected in a large increase in the blocking temperature to above 270K (Figure 9d).

However, using TOPO as ligand in the CoPt synthesis yields micrometer-sized aggregates, (Figure 10a), which consist of 2 nm sized CoPt nanoparticles (Figure 10b). These aggregates immediately precipitated after reaction. The supernatant had a blue color, indicating a large amount of Co−TOPO cluster formation. Chemical analysis of the

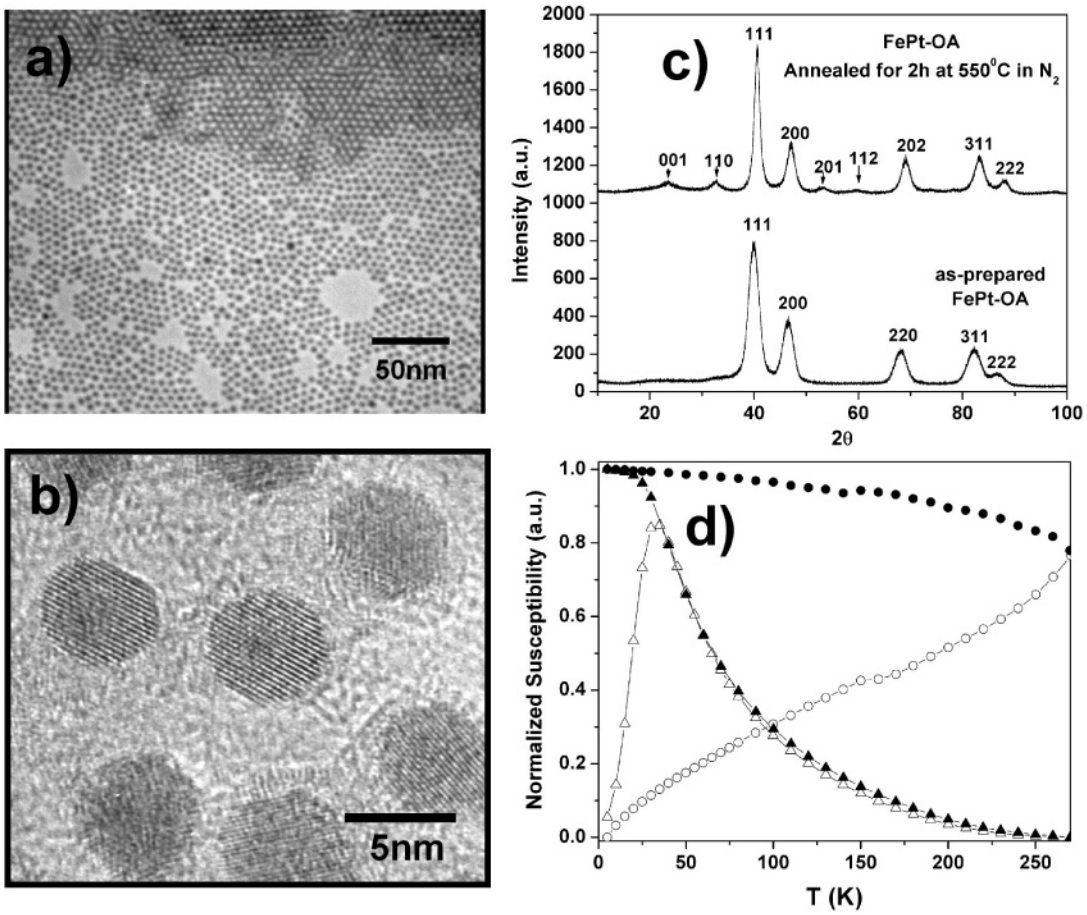

Figure 7. Monodispersed 5 nm FePt nanoparticles formed in the presence of excess OA ligand: (a) low-resolution TEM image, (b) high-resolution TEM image, (c) XRD patterns of the OA-capped FePt nanoparticles showing the fcc phase for the as-prepared sample and the fct phase for the annealed sample, (d) ZFC (open symbols) and FC (filled symbols) magnetic susceptibility curves of the as-prepared (triangles) and annealed (circles) samples.

TOPO-capped sample yields a Co:Pt molar ratio of 1:0.8, which is still less than the ratio of 2:1 in the initial precursor. The as-prepared sample exhibits broad X-ray diffraction peaks (Figure 10c), which are attributed to the predominant population of 2 nm sized nanoparticles. After annealing the nanoparticle sample at 750 °C for 2 h under an inert atmosphere, the nanoparticles sinter and X-ray diffraction shows a predominant fct phase with trace amounts of nonstoichiometric CoPt phase (Figure 10c). Due to the clustering of the 2 nm CoPt nanoparticles, the ZFC−FC susceptibility curves obtained from the as-prepared sample also exhibit a blocking temperature that is above room temperature (Figure 10d). This is in sharp contrast with the OA-ligated CoPt particles, which have a similar particle size.

The above experimental results show the growth of transition-metal and alloy particles is controlled by two competing processes: nucleation and growth of zerovalent metallic cores and a digestive mechanism to form metal cluster complexes via the ligand molecules. Both of these processes are affected by the type of ligands, metal elements involved, and concentration of the ligand present in the reaction mixture. This leads to the complex particle growth pathways that are evident in these experiments.

The binding of OA to Co and Fe is covalent in nature, forming carboxylate with a metal oxidation state of +1 and +2. However, this oxidation process is slower than metal core nucleation and growth induced by thermal decomposition of the metal carbonyl, especially at high temperature. This is confirmed by the immediate color change to black upon injection of the metal carbonyl (i.e., an indication of large clusters or nanosize particle formation). The oxidation process that follows is controlled by the concentration of OA ligand. A high concentration of OA ligand favors complete breakdown of the metal core and subsequent formation of cluster complex species (Figures 1 and 2). This process may occur at defect sites or at corner and edge sites of the metal nuclei. Furthermore, it is interesting to note that the Fe−OA and Co−OA clusters species exhibit a similar structure, which consists of two or three metal centers ligated to two or three OA molecules. These observations imply a preference for unique metal cluster sizes and ligand coordination. At a low concentration of OA there are simply not enough OA molecules to coordinate with all the metal atoms if they all exist in small cluster form. Thus, only part of the Fe and Co are oxidized and dissolved in the solution as carboxylate clusters, and the remaining metals exist in a zerovalent state that continuously grows into large zerovalent metallic nanoparticles.[20,22] Some OA molecules attached to the surface of nanoparticles and form covalent bonds with the metal.[23−26] A similar mechanism exists in the Au−dodecanethiol system which limits the nanoparticle size in

(24) Nakamoto, K. *Infrared and Raman Spectra of inorganic and coordination compounds*; John Wiley & Sons: New York, 1997.

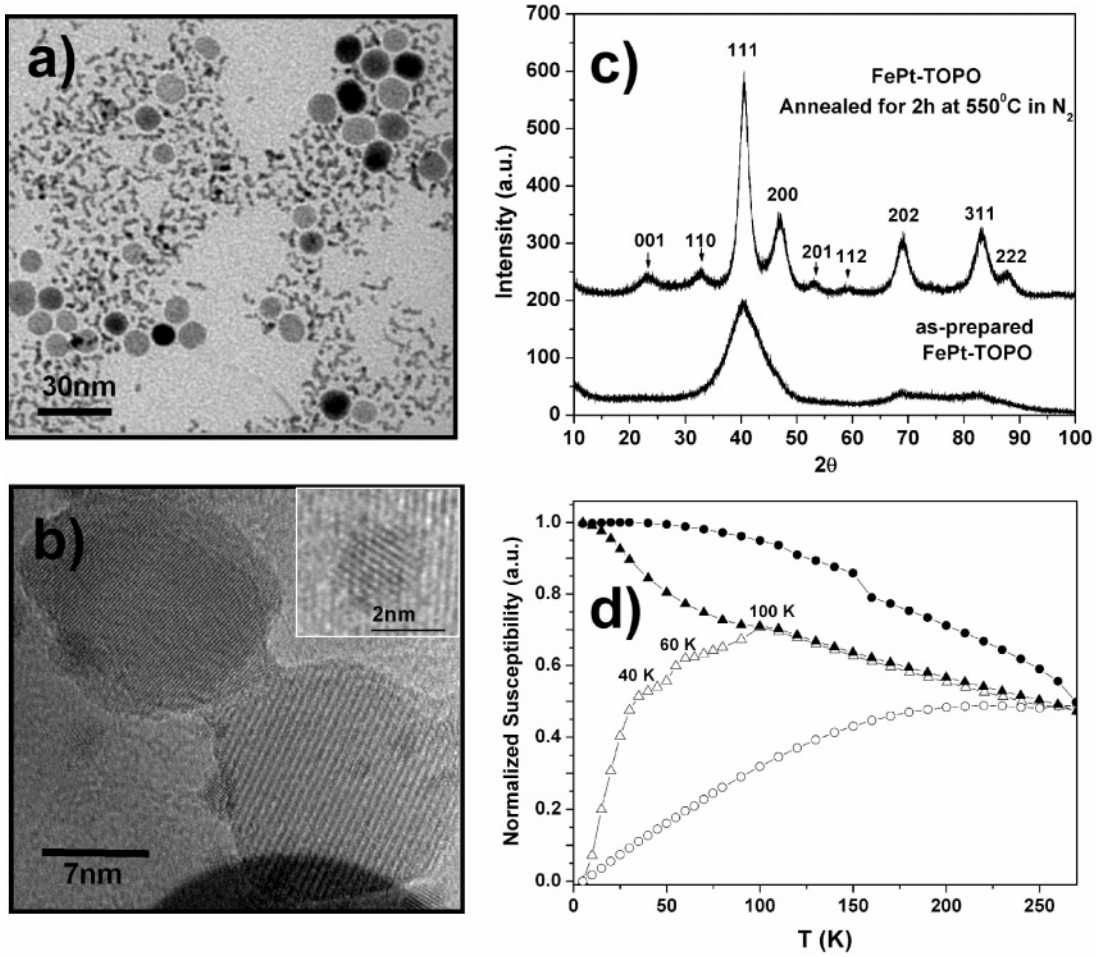

Figure 8. Bimodal distribution of FePt nanoparticles formed in the presence of excess TOPO ligand: (a) low-resolution TEM image, (b) high-resolution TEM image, (c) XRD patterns of the TOPO-capped FePt nanoparticles showing the fcc phase for the as-prepared sample and fct phase for the annealed sample, (d) ZFC (open symbols) and FC (filled symbols) magnetic susceptibility curves of the as-prepared (triangles) and annealed (circles) samples.

the size range of 5−8 nm at low temperatures (∼120 °C)[27,28] and leads to complete transformation to small thiolated cluster complex at high temperatures (∼300 °C).[29] Digestion of metal cores into small cluster complexes under a high concentration of ligand is a ripening process that is intrinsically different from the Ostwald ripening process. For the Ostwald ripening process to occur in a colloid the monomers (atoms or small clusters) are energetically unfavorable to exist as isolated species in solution and evolution of particle size is determined by the interfacial energy of the growing particles. In the digestive ripening process the cluster complexes formed are energetically favored to exist in solution due to strong binding between the metal center and ligand molecules and large solvation energy of the ligand molecules.

We need to point out that even with a high OA ligand concentration both higher reflux temperature and longer duration of reflux tend to decrease the overall concentration of oleic acid in the reaction mixture eventually due to its low boiling point (194 °C). This subsequently leads to metal oxide nanoparticles formation. In our experimental setup the Fe−oleate cluster complex is able to sustain reflux heating at 286 °C for more than 2 h. Upon continuous heating for 7 h, iron oxide particles of 12 nm (mainly in Fe_3O_4 phase) would form. On the other hand, cobalt−oleate cluster complex can sustain continuous heating at 265 °C for 7 h without color change, but cobalt oxide particles eventually form after being heated for 14 h. This is consistent with the results published earlier that oxide particles form under high temperature (>300 °C) decomposition of iron−oleate and cobalt−oleate, although the oleates are prepared through slightly different procedures than our work here.[30,31]

Compared with Co and Fe, nucleation of metal cores is more favorable than oxidation to cluster complexes for the Pt−OA system, although Pt−oleate does form on the growing nanoparticle surface, which is evident from the FTIR data (Figure 3b). This observation is consistent with the recent findings of Shevchenko et al., who reported that reduction of $Pt(acac)_2$ in the presence of 1-adamantanecarboxylic acid ligand led to bulk Pt precipitation.[11] The fact

(25) Stahl, B.; Gajbhiye, N. S.; Wilde, G.; Kramer, D.; Ellrich, J.; Ghafari, M.; Hahn, H.; Gleiter, H.; Weissmüller, J.; Wurschum, R.; Schlossmacher, P. *Adv. Mater.* **2002**, *14*, 24−27.
(26) Howard, L. E. M.; Nguyen, H. L.; Giblin, S. R.; Tanner, B. K.; Terry, I.; Hughes, A. K.; Evans, J. S. O. *J. Am. Chem. Soc.* **2005**, *127*, 10140.
(27) Lin, X. M.; Sorensen, C. M.; Klabunde, K. J. *J. Nanoparticle Res.* **2000**, *2*, 157−164.
(28) Prasad, B. L. V.; Stoeva, S. I.; Sorensen, C. M.; Klabunde, K. J. *Chem. Mater.* **2003**, *15*, 935−942.
(29) Jin, R. C.; Egusa, S.; Scherer, N. F. *J. Am. Chem. Soc.* **2004**, *126*, 9900−9901.
(30) Jana, N. R.; Chen, Y.; Peng, X. *Chem. Mater.* **2004**, *16*, 3931−3935.
(31) Park, J.; An, K.; Hwang, Y.; Park, J.-G.; Noh, H.-J.; Kim, J.-Y.; Park, J.-H.; Hwang, N.-M.; Hyeon, T. *Nat. Mater.* **2004**, *3*, 891−895.

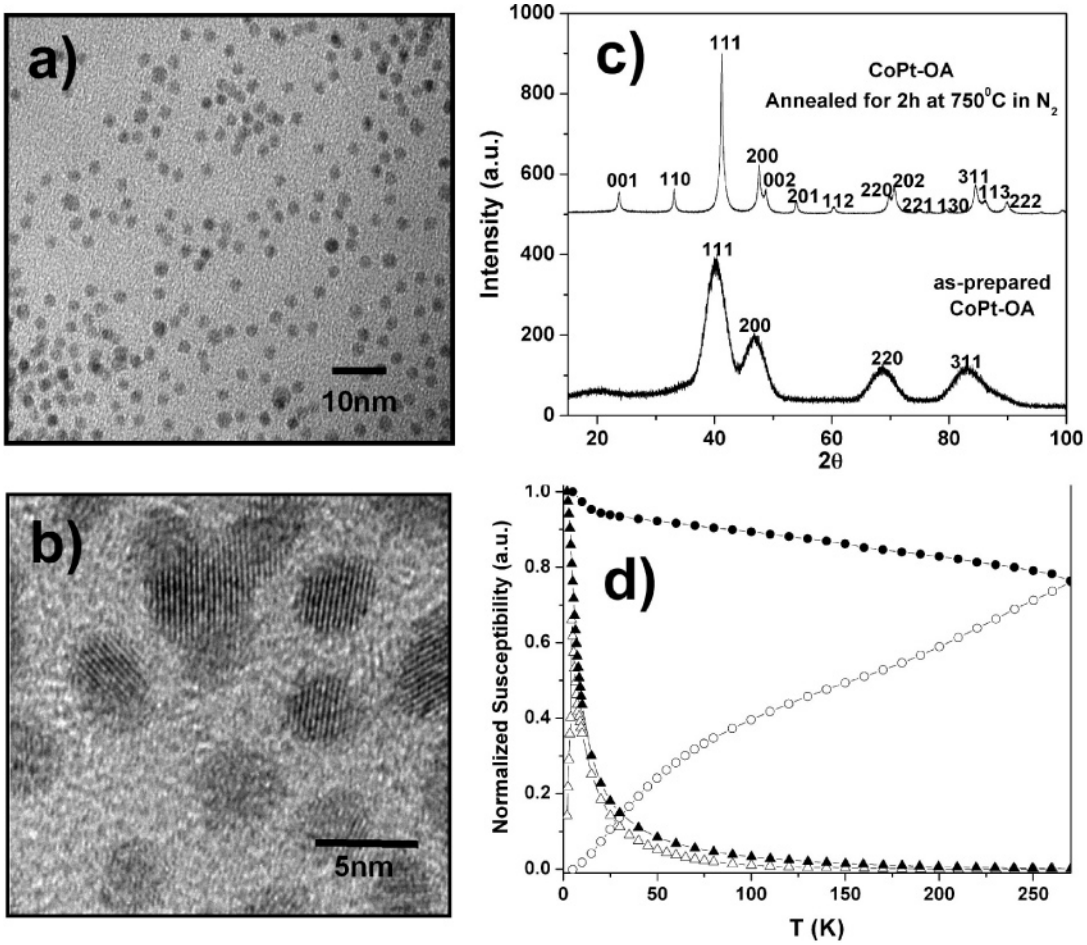

Figure 9. Monodispersed 2 nm CoPt nanoparticles formed in the presence of excess OA ligand: (a) low-resolution TEM image, (b) high-resolution TEM image, (c) XRD patterns of the OA-capped CoPt nanoparticles showing the fcc phase for the as-prepared sample and the fct phase for the annealed sample, (d) ZFC (open symbols) and FC (filled symbols) magnetic susceptibility curves of the as-prepared (triangles) and annealed (circles) samples.

that cluster complexes do not form for Pt is because it is much more difficult to oxidize than Fe and Co (oxidation potential 0.28 V for Co, 0.44 V for Fe, and −1.20 V for Pt).

The binding strength of TOPO with the transition-metal surface is weaker than with OA because the bond involves sharing a lone pair of electrons on the oxygen atom. Thus, metallic Fe and Pt core are able to grow in the environment of excess TOPO (Figures 5 and 6) to form nanometer size particles. Only cobalt still forms clusters with TOPO (Figure 4). Even for the case of Co, the mass distribution of the cluster complex is much broader and a significant amount of Co exists in the zero valence state in the clusters.

Simultaneous reduction and thermal decomposition of metal precursor leads to alloy particle formation.[32] Both the XRD data and the high-resolution TEM images of our FePt and CoPt nanoparticles indicate formation of well-mixed alloy particle instead of particles with a core−shell structure or form particles that are phase separated. Formation of alloy particles in the environment of excess OA reflects the competition between formation of metallic alloy core and the tendency for Co or Fe to form cluster complex species during the same time (Figure 11). It is likely when Fe and Co are alloyed with Pt they become less susceptible to digestion. Ligand binding on the alloy nanoparticles surface, which mainly occurs at the Co and Fe sites, begins to limit and eventually arrest the particle growth. Thus, for OA-ligated FePt and CoPt particles, growth of the particles tends to stop at a finite size (5 nm for FePt and 2 nm for CoPt). The Ostwald ripening process does not persist beyond this point. In order to generate alloy nanoparticles with a Fe(Co):Pt molar ratio close to 1:1, the concentration of Fe and Co used in the precursor has to be higher than that of Pt (in our case 2:1) because part of Co or Fe from the thermal decomposition are inevitably consumed in the formation of small cluster complexes in the solution. In most cases, these small cluster complexes are removed during the solvent washing steps. Thus, the Co and Fe content in the final nanoparticles is typically much less than in the precursors.

Formation of CoPt in an environment with excess TOPO is similar to alloy particle formation with OA. The Co:Pt ratio in TOPO-ligated CoPt nanoparticles (1:0.8) is less than the same ratio in the precursors. Also, the supernatant solution has a bluish color indicating that cluster formation occurs simultaneously with particle growth. In contrast, chemical analysis of the TOPO-ligated FePt nanoparticles reveals a Fe:Pt molar ratio of 1:0.6, which is much closer to the corresponding ratio of the initial precursors. This is because Fe does not form a cluster complex with TOPO and both Fe and Pt participate only in particle formation.

(32) Zhou, S.; Varughese, B.; Eichhorn, B.; Jackson, G.; Mcilwrath, K. *Angew. Chem., Int. Ed.* **2005**, *44*, 4539−4543.

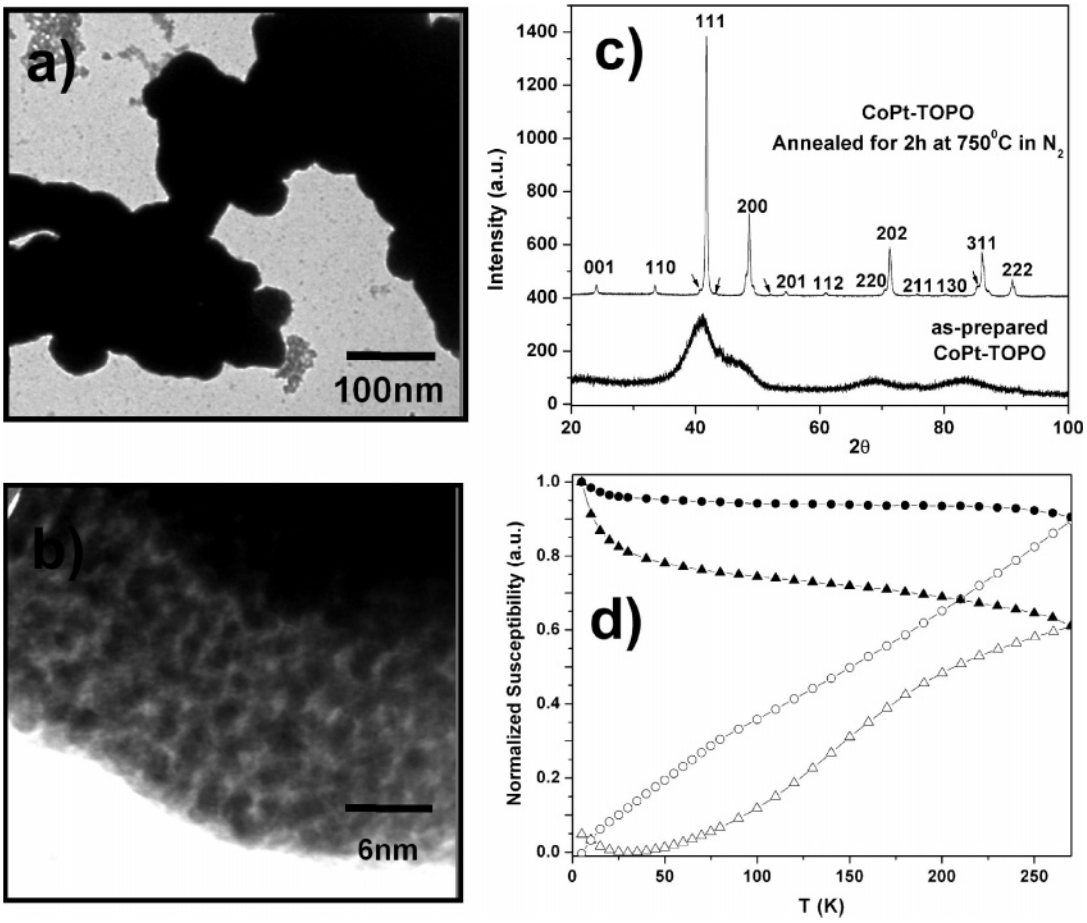

Figure 10. Aggregates of 2 nm CoPt nanoparticles formed in the presence of excess TOPO ligand: (a) low-resolution TEM image, (b) high-resolution TEM image, (c) XRD patterns of the TOPO-capped CoPt nanoparticles showing the fcc phase for the as-prepared sample and the fct phase for the annealed sample (small arrows show diffraction peaks from a small amount of nonstoichiometric CoPt phase), (d) ZFC (open symbols) and FC (filled symbols) magnetic susceptibility curves of the as-prepared (triangles) and annealed (circles) samples, respectively.

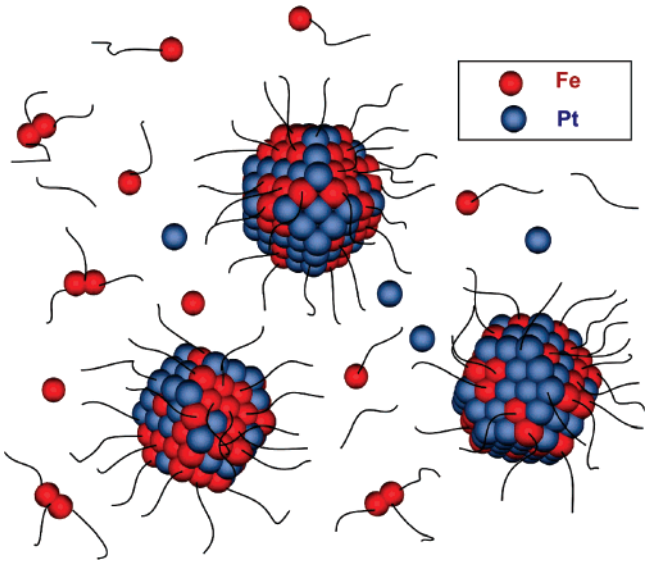

Figure 11. Schematic diagram of cluster−complex formation in bimetallic FePt nanoparticles synthesis. Because of the large amount of FeOA and Fe_2OA_3 cluster formation, the Fe:Pt molar ratio of the FePt nanoparticles is much lower than the same ratio in the precursors.

For both the Fe−TOPO and Co−TOPO systems small alloy particles (2 nm) form. However, the attractive interactions between these particles are strong enough to induce aggregation due to the short chain length of TOPO. In the case of FePt−TOPO there is a coalescence growth mode which results in a bimodal distribution of particles (2 and 14 nm) (Figure 8).[33] The intermediate stage of finite clusters of the 2 nm particles is visible in electron micrographs (Figure 9a). As a result, the ZFC magnetic susceptibility curve for the as-prepared sample shows several kinks at 40, 60, and 100 K, indicative of collective switching of the clusters. In the case of CoPt−TOPO the ligand is more strongly bound to the surface, which prevents the coalescence process from occurring. Thus, only large aggregates of 2 nm particles form without visible sintering. A strong coupling between the 2 nm nanoparticles in these aggregates causes the thermal-induced switching of magnetic moments to occur only at very high temperatures. This explains the fact that even the as-prepared sample has a blocking temperature above room temperature (Figure 10d). This is in sharp contrast with the magnetic switching behavior of the CoPt−OA sample with a similar particle size (Figure 9d).

Conclusions

In summary, we studied the effects of two different ligands (OA and TOPO) on the thermal decomposition and reduction of organometallic precursors of Co, Fe, and Pt. We find that a strong binding of the ligand to the transition metals induces

(33) Zinke−Allmang, M.; Feldman, L. C.; van Saarloos, W. *Phys. Rev. Lett.* **1992**, *68*, 2358−2361.

cluster complex formation (Co−OA, Fe−OA, and Co−TOPO), especially when a high concentration of ligand is used. This process occurs via oxidation of metal centers and provides a digestive ripening mechanism that competes with Ostwald ripening during nanoparticles formation. This process significantly affects the growth kinetics, morphology, and chemical composition of transition metals and their alloy nanoparticles. As a result, the growth of alloy particles (FePt−OA, CoPt−OA, and CoPt−TOPO) is limited in size and the Fe and Co content in the final alloy particles is typically lower than that of the precursors. In contrast to OA-capped alloy particles, CoPt−TOPO and FePt−TOPO particles also tend to aggregate. The latter system apparently has a coalescence growth mode that results in a bimodal size distribution.

Acknowledgment. We thank Peter Zapol for his help on computer graphics. TEM studies were carried out at the Electron Microscopy Center (EMC) at Argonne National Laboratory. This work was supported by DOE, BES-Materials Sciences, under Contract W-31-109-ENG-38, and the University of Chicago−ANL Consortium for Nanoscience Research (CNR).

CM0610579